Fluid hammer with gas desorption in a liquid–filling tube: experiments with three different liquids

Article *in* Experiments in Fluids · September 2015

DOI: 10.1007/s00348-015-2043-2

CITATION
1

READS
28

5 authors, including:

Marcos Lema
University of A Coruña
23 PUBLICATIONS **61** CITATIONS
SEE PROFILE

Fernando López Peña
University of A Coruña
113 PUBLICATIONS **311** CITATIONS
SEE PROFILE

Jean-Marie Buchlin
von Karman Institute for Fluid Dynamics
200 PUBLICATIONS **1,037** CITATIONS
SEE PROFILE

Johan Steelant
European Space Agency
223 PUBLICATIONS **1,278** CITATIONS
SEE PROFILE

Postprint of the research article published in Experiments in Fluids, September 2015, 56:180.
The final publication is available at www.springerlink.com
DOI 10.1007/s00348-015-2043-2

Fluid hammer with gas desorption in a liquid-filling tube: experiments with three different liquids

Marcos Lema[1] · Fernando López Peña[1] · Patrick Rambaud[2] · Jean-Marie Buchlin[2] · Johan Steelant[3]

Abstract The opening of a fast valve followed by a f uid line with a closed end generates a f uid hammer that may involve several multiphase phenomena. This is the case of the propulsion systems in satellites during the priming operation, where the lines are initially kept under vacuum conditions. The f lling with liquid propellant is done by opening a pyrotechnic valve, and the f uid hammer taking place involves cavitation and gas desorption. For this purpose, an experimental study is carried out with inert f uids modeling a liquid propulsion system, where the saturation level of the test liquid is controlled, allowing to run experiments under deaerated and saturated conditions. The results show that the f uid hammer phenomenon is affected by the gas saturation conditions if the liquid is susceptible to high desorption rate. In this case, the desorbed pressurant gas in the lines cushions the liquid front impact at the closed ends, leading to a lower pressure rise during f uid hammer occurrence.

Marcos Lema
marcos.lema@udc.es

Fernando López Peña
f op@udc.es

Jean-Marie Buchlin
buchlin@vki.ac.be

Johan Steelant
Johan.Steelant@esa.int

[1] Universidade da Coruña, Mendizábal s/n, 15403 Ferrol, Spain

[2] von Karman Institute for Fluid Dynamics, Chausse de Waterloo, 72, 1640 Rhode-Saint-Genèse, Belgium

[3] European Space Agency, Keplerlaan 1, P.O. Box 299, 2200 AG Noordwijk, The Netherlands

1 Introduction

Fluid hammer is described as a pressure surge caused by the sudden velocity change of a f uid in motion, in which the fast closure of a valve or simply a closed end in the pipeline changes the f ow conditions. The resulting pressure rise can be particularly hazardous when the pressurized liquid is discharged by fast opening a valve into an evacuated piping line, which induces a high acceleration of the f ow before going to rest at the closed end. This is the case of propulsion systems used in satellites during priming operation.

In a liquid-propellant engine, the fuel is stored in a tank, and when thrust is needed, a non-condensable gas (NCG), such as nitrogen or helium at high pressure, forces the fuel into the combustion chambers. The liquid propulsion systems are initially inactive, i.e., the propellant lines are vacuum-pumped and the tanks are isolated from the combustion chambers by three levels of isolation valves. Such a conf guration with three safety levels is a requirement during on-ground manipulation and launch operation, where all the valves are kept closed. Once the satellite has been ejected from the launcher, the activation of the spacecraft propulsion systems starts with the priming operation, which f lls the lines with the pressurized liquid propellant stored in the tanks. Priming is done by fast opening a pyrotechnic isolation valve, allowing the liquid propellant to f ow into the evacuated propellant lines.

This conf guration generates a f ow with the presence of several phases from the moment that the f uid encounters vacuum conditions, even before the f uid hammer takes place. In particular, the driving pressure gas dissolves in the liquid during storage in the tanks. When the valve opens, the new pressure conditions are below the saturation pressure, inducing the desorption of the NCG, which is known

as gaseous cavitation (Bergant et al. 2006). The additional gas phase comes from the cavitation of the liquid when the pressure conditions in the line are below the vapor pressure, which is known as vaporous cavitation (Bergant et al. 2006).

The f uid f owing in the line under vacuum conditions is suddenly decelerated by a closed end, which induces the f uid hammer considered in the present study. That leads to a pressure surge that exceeds several times the initial pressure in the tank and that might damage the piping system. Nowadays, the assessment of piping systems undergoing pressure transients relies on numerical simulations, and the numerical models used are established on the basis of results obtained with water in simple conf gurations. They are able to accurately predict the effects of liquid compressibility when computing a single-phase f uid hammer, but they still need to be extended and calibrated for cases with cavitation (single-component) and two-phase (two-component) f ows. There are very few literature references describing experiments with all the specif cations of the above conf guration of propulsion systems (f uid hammer, cavitation, absorption, desorption), usually with a poor description of the test conditions (Yaggy 1984; Prickett et al. 1992; Ounougha and Colozzi 1997; Leca and Boh 2000; Molinsky 1997; Morgan 2004), so that a proper validation of the physical models implemented in numerical tools is still missing. To do so, the creation of an extensive database concerning the previously described conf guration is necessary for the improvement in these numerical tools.

The objective of this paper is to study experimentally the f uid hammer phenomenon in a conf ned environment modeling a spacecraft propulsion system. For this purpose, an experimental facility is designed and built, to be run with inert f uids instead of highly toxic liquid propellants. Characterization of the variables of the problem and their inf uence on the pressure surges, covering aspects such as initial vacuum conditions in the line, liquid properties, pipe conf gurations, and liquid saturation conditions are addressed in the parametric study.

2 Experimental facility

The experimental facility built for the present study includes all the elements of a satellite propulsion system directly involved in the f uid hammer occurrence, i.e., a pressurized liquid tank, a fast opening valve (FOV), and a given length of pipe line. The main objective during the design phase was to conceive a facility without singular elements such as elbows and T-junctions upstream of the FOV, and with the same inner diameter in every piping element. It is well known that these geometrical singularities create secondary pressure waves, which complicate the general pressure measurements interpretation. The facility is intended to be run with inert f uids and nitrogen as driving pressure gas.

The facility layout is presented in Fig. 3, which is clamped onto a vertical wall. The main components are a pressure vessel, a valve with an opening time lower than 40 ms and a 2 m length propellant line, referred to as “test element”. The facility also includes a vacuum system to set the test conditions in the propellant line, as shown in Fig. 3.

The test elements are made with the same titanium tube used for aerospace applications (alloy T3AL2.5V, specif cation AMS4943H), with 0.25 in. (6.35 mm) of inner diameter and 0.016 in. (0.4 mm) thickness (Fig. 1). The test elements are anchored to the facility platform by using the same supports used in satellites. Figure 2 shows the support assemblage, leaving a separation of 83 mm between the tube and the platform. The supports are spaced by 250 mm, which is the same construction rule followed in satellite construction.

Fig. 1 Titanium tube used to build the test elements

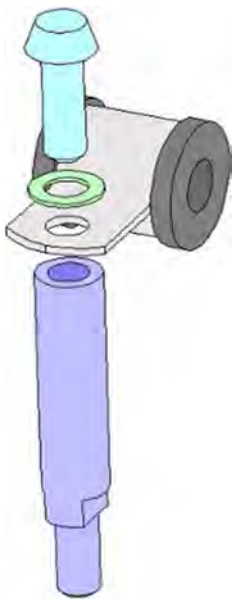

Fig. 2 Test element support used to anchored the tubes

The most critical element of the facility is the FOV. Pyrotechnic type valves are used for the priming process in satellites for their reliability, but with opening times in the vicinity of 5 ms. For practical reasons, these valves are avoided in parametric studies and a ball valve with a pneumatic actuator is used instead, resulting in opening times of around 40 ms. It is believed that this value is fast enough to experience a rise in pressure similar to the one obtained with a pyrotechnic valve. This point has been stated by several authors (Yaggy 1984; Prickett et al. 1992; Lin and Baker 1995) and also verif ed experimentally in the present study.

A measurement module is attached at the bottom end of the test section, as highlighted in Fig. 3. This is the impact location of the liquid front and where the f uid hammer is originated. This module, made of stainless steel and drilled with the same inner diameter as the propellant line, allows the unsteady measurements of pressure with a dynamic transducer f ush mounted at the bottom end wall, as presented in Fig. 4.

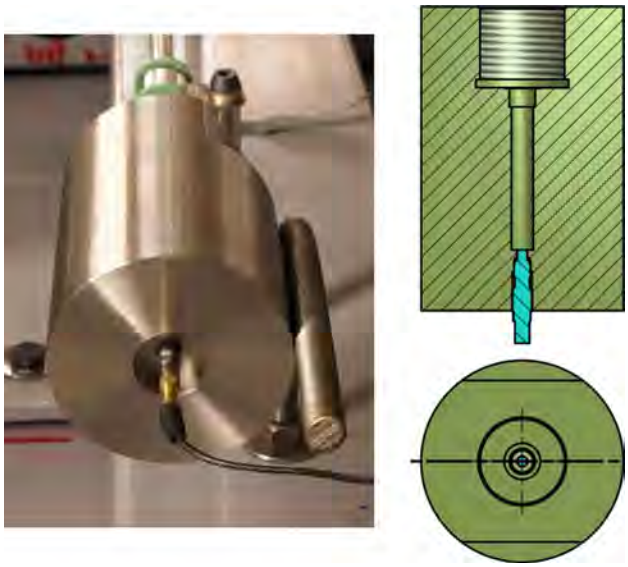

Fig. 4 Instrumented measurement module with 105C22 sensor

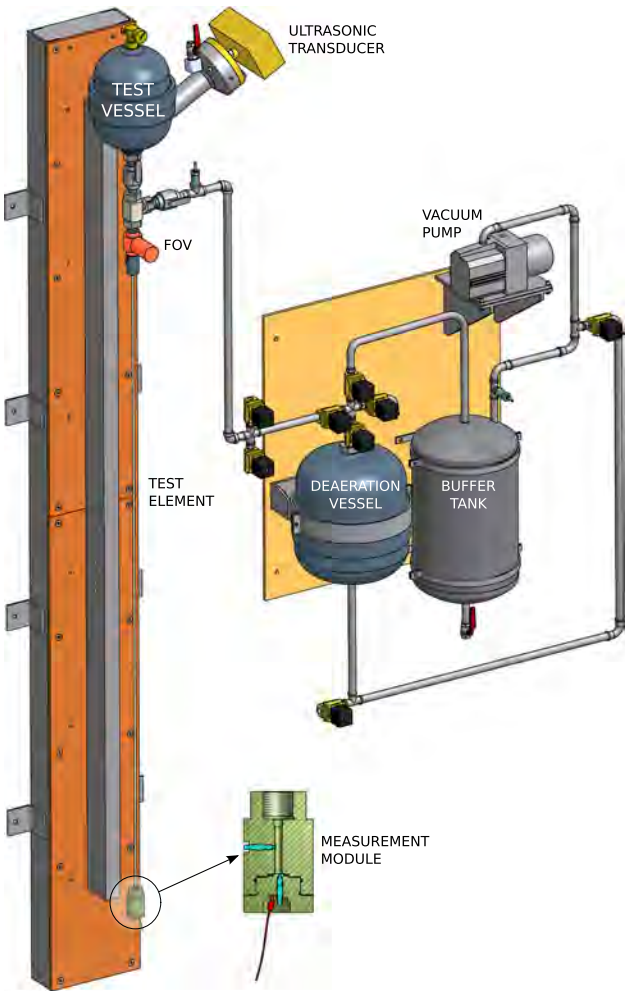

Fig. 3 Experimental facility layout

The test vessel is a spherical accumulator that can mount an elastic membrane, and it is equipped with an ultrasonic transducer to measure the speed of sound in the liquid. The purpose of the membrane is to avoid the absorption of the NCG during the liquid pressurization, allowing to run experiments with deaerated or fully saturated liquid. This test procedure will allow to understand how the dissolved gas affects the f uid hammer mechanism. In order to run experiments under deaerated conditions, any gas dissolved in the test liquid needs to be removed. This is done by means of a depressurization process using a second accumulator, called deaeration vessel, connected to the vacuum pump, both shown in Fig. 3. The dissolved gas is removed by keeping the liquid in a low-pressure atmosphere. The deaeration vessel also mounts an elastic membrane in order to transfer the deaerated liquid into the test vessel using compressed air, without any contact between the two phases.

Regarding the test procedure, it starts by f lling the tank with the working liquid to be later pressurized by means of compressed NCG. The facility is ready for a test when the propellant line is vacuum-pumped, the FOV closed, and the pipe segment between the tank and the FOV f lled with the pressurized working liquid. The f uid hammer events start by opening the FOV and take place when the liquid hits the closed end.

The experimental database is built upon the main parameters that can be varied experimentally: test liquids (water, ethanol, and acetaldehyde), the vacuum conditions in the tube, and the liquid saturation with NCG (fully deaerated

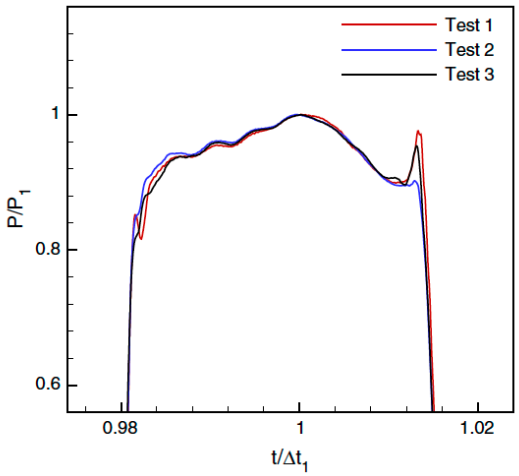

Fig. 5 Test repeatability obtained in the f rst pressure rise

or saturated). The test element conf guration used is 2.00 m straight, and the pressure in the tank is kept constant and equal to 2 MPa. Measurements for every test condition shown hereafter have been repeated three times, in order to ensure test repeatability. Figure 5 shows the repeatability of the f rst pressure rise during f uid hammer occurrence for three tests under the same initial conditions (deaerated water, $P_T = 2$ Mpa and $P_p = 1$ kPa).

3 Test liquids

Three liquids are used in this study instead of real propellants, such as monomethylhydrazine (MMH) and nitrogen tetroxide (NTO), both commonly used as hypergolic propellant combination in rocket engines, which manipulation involves expensive safety precautions. Table 1 summarizes the physical properties involved in f uid hammer occurrence (density, ρ, and wave velocity, c), multiphase behavior of the f ow (liquid saturation pressure, P_v, and surface tension, σ), and friction (viscosity, μ). Water has similar values of density, viscosity, and wave velocity to MMH, but with half the vapor pressure and a surface tension value twice as large. Ethanol has similar vapor pressure and viscosity values to those of MMH, and similar speed of sound and surface tension to NTO. Acetaldehyde has the closest viscosity to that of NTO, with similar vapor pressure, speed of sound and surface tension. It is worth mentioning that NTO density is higher than in any other test liquid used in this study.

3.1 Deaerated and saturated conditions

A parameter that may play an important role in the f uid hammer event is the saturation level of the working f uid with the NCG. In normal conditions, the driving pressure gas gets dissolved in the liquid through a diffusive process, and the saturation level is def ned by the pressure applied to the NCG during storage. In order to characterize the inf uence of the saturation level on the f uid hammer phenomenon, two types of experiments are def ned: fully deaerated and fully saturated liquid. In the present f ow conf guration, nitrogen is the solute, and the solvents are the three test liquids.

The deaerated condition is set by applying a degasif cation process to the test liquid. This is achieved by keeping the liquid under reduced pressure, often referred to as vacuum degasif cation. This process allows reducing the gas solubility by reducing the partial pressure, and, as stated by Henry's law, a less soluble gas will desorb from the liquid + gas solution. The f nal partial pressure applied to the solution during the vacuum degasif cation is always kept slightly above the liquid vapor pressure to avoid the boiling of the liquid and the massive arrival of vapor at the vacuum pump. With the liquid fully deaerated, it is transferred to the main tank. Both the degasif cation tank and the main tank have mounted membranes to isolate the liquid side from the gas side. In this way, the liquid can be pushed toward the main tank without the contact of the driving pressure gas with the test liquid.

In case the liquid needs to be saturated with the driving pressure gas, the deaerated liquid is transferred to the tank previously f lled with the NCG, and pressure is applied to the gas side of the accumulator, above the membrane. In this way, the contact of the two phases is ensured during tank pressurization. Since saturation is based on the molecular diffusion of the two species, and due to the absence of

Table 1 Physical properties of inert test f uids and propellants in liquid phase at 293 K

	MMH	Water	Ethanol	Acetaldehyde	NTO
ρ (kg/m^3)	875	998	789	783	1447
μ (Pa s)	0.000855	0.001	0.00144	0.00023	0.0004
c (m/s)	1568	1487	1176	1141	1004
P_v (Pa)	4908	2300	5950	101,300	90,710
σ (N/m)	33.83×10^{-3}[a]	72.85×10^{-3}	22.27×10^{-3}	21.2×10^{-3}	27.5×10^{-3}

[a] Value at 298.15 K

a device to monitor the growing amount of gas dissolved in the liquid, it has been assumed that complete saturation of the liquid is achieved after 24 h. To validate this assumption, tests have been performed with water undergoing saturation conditions for more than 48 h, without observing a signif cant difference on the f uid hammer pressure levels.

Under these conditions, and in order to estimate the amount of NCG dissolved in the liquid, Henry's law can be used, as shown in Eq. 1:

$$p_{\mathrm{g}} = k_{\mathrm{H}} \cdot X_{N_2} \tag{1}$$

where X_{N_2} is the molar concentration of a species in the liquid phase, p_{g} is the partial pressure of that species in the gas phase above the liquid, and k_{H} is Henry's law constant. Sander (1999) showed a simple way to describe the Henry constant as a function of temperature in the form of the Van't Hoff equation:

$$k_{\mathrm{H}} = k_{\mathrm{H}}^{\ominus} \exp \frac{-\triangle_{\mathrm{soln}} H}{R} \left(\frac{1}{T} - \frac{1}{T^{\ominus}} \right) \tag{2}$$

in which the symbol $\ominus$ refers to standard conditions ($T^{\ominus} = 298.15\,\mathrm{K}$), R is the gas constant, and $\triangle_{\mathrm{soln}} H$ is the enthalpy of the solution, following the temperature dependence:

$$\frac{\triangle_{\mathrm{soln}} H}{R} = \frac{-\mathrm{d}lnk_{\mathrm{H}}}{\mathrm{d}(1/T)} \tag{3}$$

The solubility of nitrogen in water has been extensively studied in the articles by Wilhelm et al. (1977) and Sander (1999). Usually, the Henry constant value slightly differs among different authors and, in case of nitrogen dissolved in water, two values are equally often proposed under standard conditions, as indicated by Sander (1999). These values, together with the temperature correction and the partial pressure set for saturated and deaerated conditions, allows computing the dissolved NCG molar fraction. The computed data for nitrogen dissolved in water are summarized in Table 2, where the gas mass fraction of nitrogen is indicated in the last row.

The solubility of nitrogen in ethanol has also been studied by several authors, who proposed different empirical relations or tabulated data to compute the Henry constant or to directly get the molar fraction value. Katayama and Nitta (1976) obtained the solubilities of nitrogen for several alcohols, among them ethanol, which are expressed in terms of Ostwald's coeff cient and Henry's constant. Fischer and Wilken (2001) studied the nitrogen solubility in organic solvents and their results are given directly in terms of molar fraction for different pressures and temperatures. In these two articles there is not any temperature correction, nor the necessary data to apply Van't Hoff equation. On the other hand, Battino et al. (1984) tabulated the molar concentration of nitrogen in ethanol for a partial pressure of 1 atm and in the temperature range of 213.5–313.5 K. The authors also proposed a mathematical relation where the molar fraction is written as a function of temperature and the partial pressure of the gas, as Eq. 4 shows:

$$\ln(x) = -9.9399 + \frac{5.4296}{\tau} + 2.0716 \cdot \ln(\tau) + 0.90833 \cdot \ln(p_{\mathrm{g}}) \tag{4}$$

In this equation, the partial pressure, p_{g}, is expressed in MPa and the temperature parameter, τ, is given in K and computed as:

$$\tau = \frac{T}{100}$$

As in the case of water, the data for nitrogen dissolved in ethanol are given in Table 3, both for deaerated and saturated conditions, with the gas mass fraction indicated in the last row.

Unfortunately, the saturated and deaerated conditions for acetaldehyde cannot be presented. To our knowledge, there are not any data available in the literature describing the solubility of nitrogen in this liquid.

Table 2 Molar and mass fraction of nitrogen dissolved in water

	Deaerated		Saturated	
$k_H^{\ominus}$ $\frac{\mathrm{atm \cdot l}}{\mathrm{mol}}$	1639.34	1538.46	1639.34	1538.46
$\frac{-\mathrm{d}lnk_H}{\mathrm{d}(1/T)}$ (K)	1300	1300	1300	1300
T (K)	293	293	293	293
k_H $\frac{\mathrm{atm \cdot l}}{\mathrm{mol}}$	1518.4	1424.96	1518.4	1424.96
P_g (Pa)	2500	2500	2×10^6	2×10^6
X_{N_2} (mol/l)	1.62×10^{-5}	1.73×10^{-5}	1.30×10^{-2}	1.39×10^{-2}
M_{N_2} (g/mol)	28.02	28.02	28.02	28.02
x_{N_2} (g/l)	4.55×10^{-4}	4.85×10^{-4}	0.364	0.388
ρ_{H_2O} (g/l)	998	998	998	998
x_{N_2} (−)	4.56×10^{-7}	4.86×10^{-7}	3.65×10^{-4}	3.89×10^{-4}

3.2 Gas desorption

In a liquid + gas mixture, the gas remains dissolved unless its temperature is raised or its pressure is lowered below the saturation pressure, since both circumstances reduce the gas solubility. When gas release takes place, small bubbles come out of the solution, and they are carried by the f ow. The presence of these small bubbles is often referred to as gaseous cavitation by several authors (da Silva and de Freitas Rachid 2013; Bergant et al. 2006; Wylie and Streeter 1978), which should not be confused with vaporous cavitation, in which the liquid is transformed into vapor when the pressure falls below its vapor pressure. When wave propagation phenomena are involved, as occurs with f uid

Table 3 Molar and mass fraction of nitrogen dissolved in ethanol

	Deaerated	Saturated
T (K)	293	293
p_g (Pa)	5000	2×10^6
X_{N_2} (mol/l)	2.32×10^{-5}	5.35×10^{-3}
M_{N_2} (g/mol)	28.02	28.02
x_{N_2} (g/l)	6.49×10^{-4}	0.15
ρ_{Ethanol} (g/l)	789	789
x_{N_2} (−)	8.23×10^{-7}	1.90×10^{-4}

hammer, the presence of entrained gas in suspension in the liquid, even in very small quantities, is responsible for reducing the wave velocity in the medium and for attenuating the pressure peaks due to the added compressibility of the gas, as described by Wylie and Streeter (1978).

The derivation of gas release rate was the objective of several authors, but Kranenburg (1974) was the first to propose an expression involving the saturation pressure, the instantaneous fluid pressure, and Henry's constant of solubility. This expression is very complex due to the uncertainties involved, but it was reduced to a more pedagogical expression by Wylie and Streeter (1978):

$$\dot{m} = C_K(P_{\text{sat}} - P) \tag{5}$$

in which $\dot{m}$ is the mass rate of gas release, P_{sat} is the saturation pressure, and P is the liquid pressure. The factor C_K is a function of the solubility coefficient, the initial void fraction of dissolved gas, the level of molecular agitation, and many other parameters. Focusing on the level of agitation, this is related to the type of molecules that make up the liquid, and the intermolecular forces between them. If the forces are relatively strong, a low level of agitation is expected, which can be linked to a low gas desorption mass rate. On the contrary, relatively weak forces will result in a higher level of agitation, and a higher mass rate of gas release may be expected. It is worth mentioning that the intermolecular forces are also related to the vapor pressure of the liquid and the surface tension, as described in the classical text book of physical chemistry by Castellan (1983). For instance, the high vapor pressure of acetaldehyde is related to the weak dipole–dipole forces and London dispersion forces between molecules. On the other extreme, water has a strong hydrogen bonding between molecules, where each molecule can potentially form four hydrogen bonds with surrounding water molecules. This is the reason of liquid water's high boiling point and low vapor pressure. Hydrogen bonding can also occur between ethanol molecules, although not as effectively as in water, since in the ethanol molecule there is only one hydrogen for the bonding to occur. Therefore, based on this information, it can be expected that under the same pressure conditions acetaldehyde undergoes a higher desorption rate than ethanol, and ethanol higher than water.

4 Results

4.1 Uncertainty analysis

The uncertainty analysis of the experimental measurements is first introduced in the present section. Following the recommendations of the book by Dieck (2007), and the article by Kline and McClintock (1953), together with the methodology proposed by the ASME (Abernethy et al. 1985), the uncertainty analysis is divided into the computation of the accuracy or bias, and the precision. Once these values are known, the uncertainty can be easily obtained by solving Eq. 6.

$$U = \overline{B^2 + P^2} \tag{6}$$

The measuring techniques basically consist of a measurement module with an unsteady pressure transducers. The measuring chain of the unsteady pressure signal includes a piezoelectric transducer, a signal conditioner with an integrated low-pass filter at 50 kHz, and the

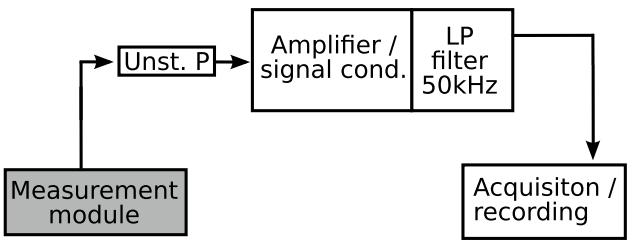

Fig. 6 Pressure measurement chain

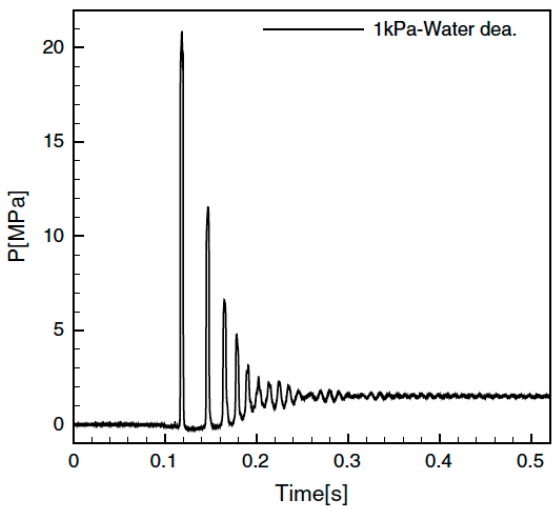

Fig. 7 Pressure evolution at the bottom end

Table 4 Uncertainty calculation

	PCB 105C22		Validyne 1 bar	Validyne 20 bar
Calibration curve	$P = C \cdot U$	Calibration curve	$P = P_{atm} \pm C \cdot U$	
C (MPa/V)	6.8918	C (Pa/V)	10,000	4×10^5
ΔC (%)	1.3	Range (V)	10	5
Range (V)	10	ΔU (V)	±0.01	±0.01
Filter error (%)	0.2	ΔP_{ref} (Pa)	±10	±100
A/D error (%)	0.02	ΔC (Pa/V)	10.05	800.2
ΔU(V)	±0.022	ΔP_{atm} (Pa)	±1	±1
Accuracy (MPa)	0.793	Accuracy (Pa)	141.7	5657
Precision (MPa)	0.3955	Precision (Pa)	–	–
Uncertainty (MPa)	0.886	Uncertainty (Pa)	149.7	5721

acquisition module, as sketched in Fig. 6. The sampling frequency is set at 150 kHz and each measurement has a duration of 1.5 s, which results in 225,000 sample points per experiment.

Regarding the steady measurements, membrane pressure transducers are used to set the initial test conditions in the tank and in the evacuated line. The first transducer has a pressure range of 0–2 MPa, with the positive port connected to the tank and the negative port left opened to the atmosphere. The second pressure transducer is configured to measure vacuum conditions. Therefore, the pressure range is 0–100 kPa, with the negative port connected to the vacuum system and the positive port left opened to the atmosphere.

Table 4 summarizes the necessary data to compute the uncertainty of each measured variable. In case of the unsteady pressure transducers, all the data are provided by the manufacturer. The "filter error" refers to the error in the signal conditioner and includes the amplifier and the low-pass filter. The "A/D error" refers to the error in the analog-to-digital converter of the acquisition card. The membrane pressure transducers have been calibrated before each test session, and the calibration data are also given in Table 4.

4.2 Pressure measurements

The analysis of the results is based on the pressure signal obtained at the closed end, at the liquid front impact location. A typical pressure measurement is presented in Fig. 7, showing the fluid hammer taking place when deaerated water flows in the straight line evacuated at 1 kPa. The reference time in the graph (i.e., $t = 0$ s) is set by the trigger of the acquisition system, which also sends the signal to the pneumatic actuator to open the FOV. The process to open the valve can be rather long, since it starts with the opening of the solenoid valve at the inlet port of the pneumatic actuator. Later, the actuator starts to move to complete the 90° turn, although the valve starts to effectively open after covering the first 45°. Therefore, the initial delay of

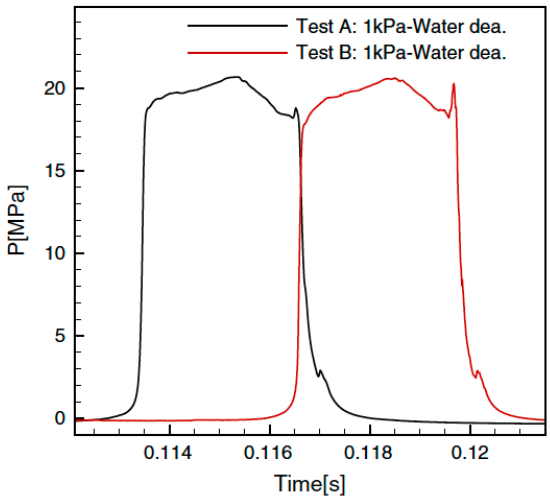

Fig. 8 First peak time occurrence comparison

approximately 0.1 s observed in Fig. 7 before the appearance of the first pressure surge includes the complete valve opening sequence and the liquid front traveling before reaching the measurement module. Unfortunately, the opening of the valve induces an error in the timing of the first peak appearance. In particular, two consecutive experiments, under the same test conditions, show different time occurrences for the first pressure peak, as shown in Fig. 8. There are several explanations to this behavior, and most probably, the answer is a combination of all of them: CPU load of the acquisition computer, temperature of the electronics, variation of the air pressure feeding the pneumatic system, temperature of the electromagnetic valve, change on the ball valve lubrication conditions, etc. All these variables are difficult to control, and the best solution would have been to use a time reference linked to the effective valve movement, i.e., acquisition starts when the pneumatic actuator has turned the valve shaft 45°. Therefore, the analysis of the results involving the time occurrence of the first pressure rise has to be performed carefully.

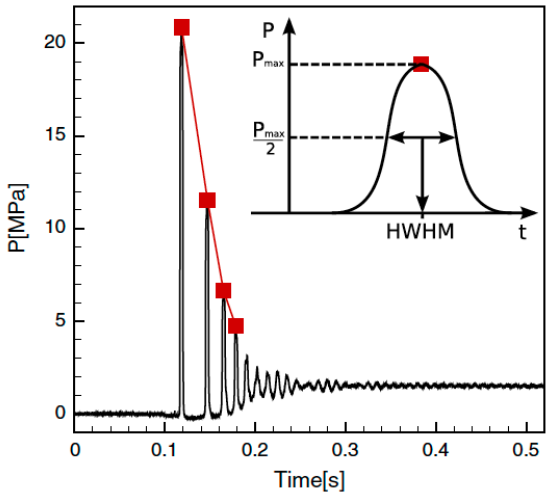

Fig. 9 Pressure evolution and HWHM def nition

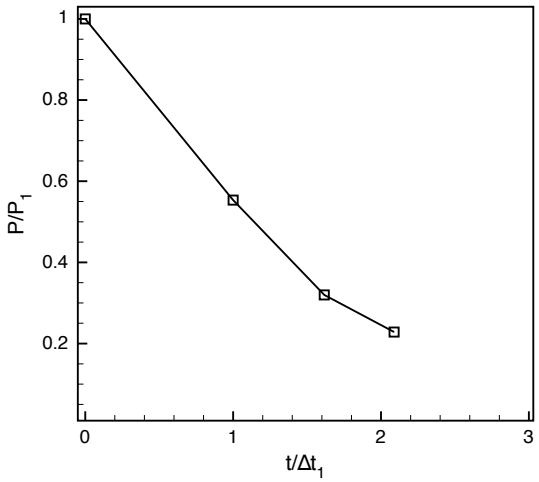

Fig. 10 Dimensionless pressure signal attenuation

Also regarding Fig. 7, even if the acquisition time has been set to 1.5 s for all the experiments (only 0.5 s plotted in this graph), the pressure signal is attenuated long before reaching this time.

4.3 Pressure signal attenuation

Together with the time-dependent evolution, the pressure peaks amplitude and time occurrence for the f rst four peaks are highlighted to compare different test conditions, as indicated in Fig. 9 with square symbols. The time occurrence of each peak is determined with the half width at half maximum (HWHM). To do so, the full width at half maximum (FWHM) is def ned as the distance between the two points of the peak at which the pressure reaches half of its maximum value. Then, the HWHM is just half of the FWHM, which gives the peak location on the time axis, as illustrated in Fig. 9.

In Fig. 10, the peak amplitude versus time occurrence is presented in dimensionless form, where the maximum pressure level reached at each peak is divided by the f rst pressure surge (P_1), and the time occurrence by the time delay between the f rst and the second peak ($\Delta t_1 = t_2 - t_1$), which is the longest time delay taking place between peaks. The dimensionless representation of Fig. 10 shows how the attenuation process is characterized by lowering peak pressure, accompanied by a continuous decrease in the time delay between peaks. This means that the largest time delay takes place between the f rst and second peaks, and it gets shorter in successive pressure peaks. This representation will allow to analyze the pressure signal decay and to compare easily different test conditions.

4.4 Results with water

While the pressure in the tank is kept constant and equal to $P_T = 2$ MPa, two pressure levels are used as initial conditions in the line: $P_p = 1$ kPa and $P_p = 10$ kPa. These two values allow setting initial conditions below and above the vapor pressure of water (2.3 kPa).

Figure 11 shows the pressure evolution obtained with water, where deaerated and saturated conditions are compared in the same graph. The peak amplitude and time occurrence are also presented in dimensionless form in the same f gure.

The analysis of the pressure levels shows that, under deaerated conditions, the highest pressure rise takes place with the lowest initial pressure in the line, i.e., 1 kPa. This is a consequence of the added compressibility of the residual gas left in the line, and since the amount of the initial NCG is higher when $P_p = 10$ kPa, it cushions more effectively the impact of the liquid front at the bottom end, resulting in a lower pressure rise. Furthermore, the peak levels in the graphs are nearly equal to deaerated and saturated conditions. This means that the amount of NCG coming out of solution during the f uid hammer occurrence when water is the test f uid is not large enough to have a signif cant inf uence on the pressure levels.

Regarding the pressure attenuation, the dimensionless graph for both deaerated and saturated conditions shows almost coincident lines. This indicates that the attenuation pattern is nearly the same without a clear inf uence of the NCG gas dissolved in the liquid. Such a behavior is an indicator that the gas desorption rate may be very low when water is the test liquid.

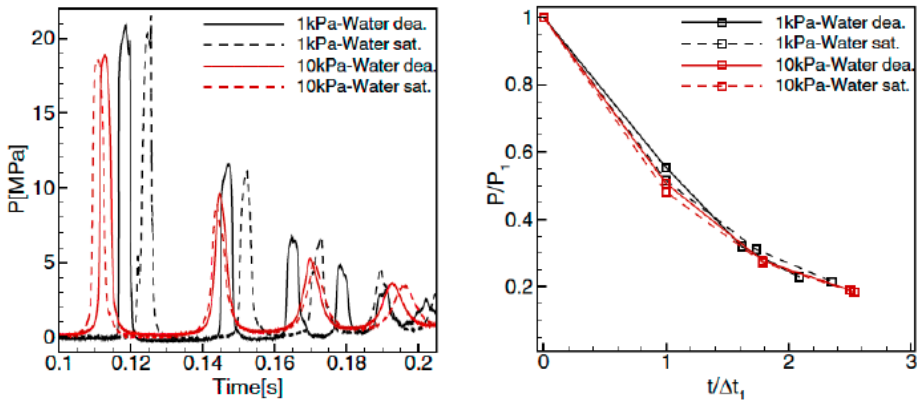

Fig. 11 Pressure evolution and dimensionless peak values obtained with water

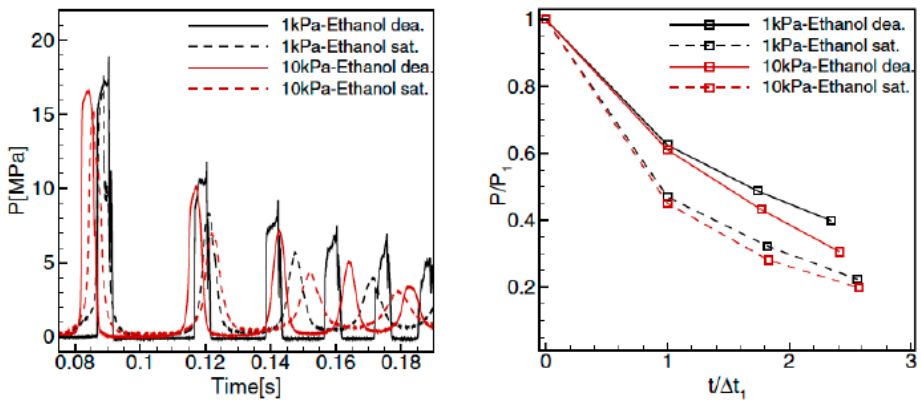

Fig. 12 Pressure evolution and dimensionless peak values obtained with ethanol

4.5 Results with ethanol

Figure 12 shows the results obtained with ethanol, both for deaerated and saturated conditions. As with water, the highest pressure rise takes place for the lowest initial pressure in the line. But this time, saturated ethanol gives lower pressure levels when compared to deaerated conditions. This fact is already observed in the first pressure peak, but the differences are even higher in successive peaks. In contrast to the results with water, the desorption rate appears to be higher with ethanol during fluid hammer occurrence and participates to increase the cushion effect of the residual gas left in the line, and to reduce the speed of sound in the liquid + gas mixture. Taking into account that the gas mass fraction of nitrogen dissolved in water for $P_T = 2$ MPa is higher than in ethanol ($x_{N_2} = 0.37$ g/l compared to $x_{N_2} = 0.15$ g/l, both values computed with Henry's law), these differences in the pressure levels show that the desorption rate must be higher in ethanol. This fact will be analyzed more in detail in the liquid comparison Sect. 4.7.

Regarding the pressure attenuation process, under deaerated conditions and when $P_p = 10$ kPa, due to a lower initial pressure rise and a higher amount of residual gas in the line that adds compressibility to the flow, the corresponding decay line tends to zero faster than that for $P_p = 1$ kPa. This behavior was already observed with water under deaerated conditions. On the other hand, under saturated conditions the signal attenuation pattern changes considerably. First of all, the attenuation process taking place when $P_p = 1$ kPa is quite similar to the one when $P_p = 10$ kPa, both under saturated conditions. This means that, due to the growing amount of evolved gas, the attenuation pattern gets closer independently of the initial residual gas in the line (the effect of the desorbed gas exceeds the importance of the residual gas on the pressure attenuation). On top of that, the signal attenuation is now stronger compared to deaerated conditions, as it is shown in the dimensionless graph in Fig. 12. An increasing amount of NCG due to a high desorption rate cushions the successive peaks and reduces the speed of sound in the mixture, reducing the pressure levels and inducing a faster pressure signal attenuation.

4.6 Results with acetaldehyde

Finally, the results with acetaldehyde are presented in Fig. 13, where once again, the highest pressure rise takes place with the lowest initial pressure in the line, as it was observed with water and ethanol. The dimensionless graph shows the same attenuation pattern as observed with ethanol; the decay line for $P_p = 10$ kPa tends to zero faster than

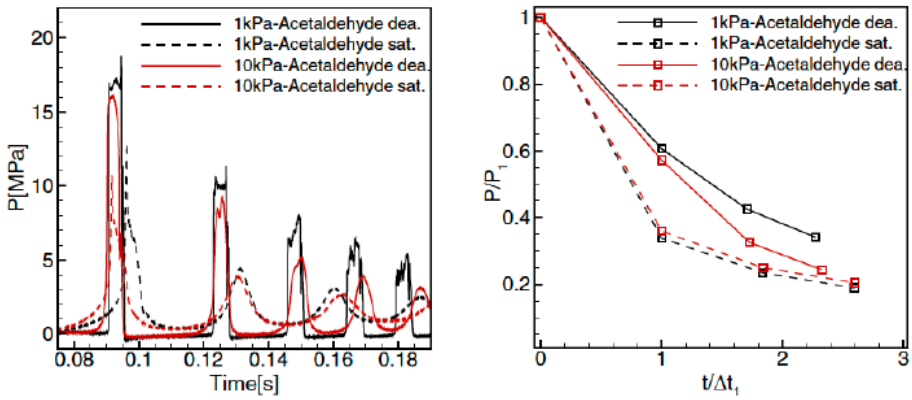

Fig. 13 Pressure evolution and dimensionless peak values obtained with acetaldehyde

that for $P_p = 1$ kPa, due to the lower initial fluid hammer pressure rise when $P_p = 10$ kPa and the added compressibility from the residual gas.

Acetaldehyde under saturated conditions is highly affected by the dissolved NCG, as can be observed in the dimensionless plot of Fig. 13. As it has already been observed with ethanol, the desorption process in acetaldehyde is fast enough to drastically increase the presence of evolved NCG, changing the fluid hammer pattern due to added compressibility and lower speed of sound. For instance, the pressure levels are now approximately 35 % lower when compared to the ones with deaerated conditions. A growing amount of desorbed NCG considerably increases the cushion effect on the pressure signal and reduces the speed of sound, something that was not observed that clearly with ethanol. Besides, the same attenuation pattern is observed when $P_p = 1$ kPa and $P_p = 10$ kPa, both under saturated conditions, showing that the whole phenomenon is driven by the massive gas desorption, independent of the initial amount of residual gas. Furthermore, due to a higher presence of evolved gas, the signal decay is also faster, as observed with ethanol, which must be again due to an increasing cushion effect and lower speed of sound induced by the evolved NCG.

4.7 Liquids comparison

Now that the results with the three liquids have been presented independently, it is worth comparing them, keeping the initial pressure in the line constant. Figure 14 shows the pressure evolution and dimensionless peak pressure decay under deaerated and saturated conditions. The results with $P_p = 1$ kPa have been plotted in the upper graphs, while the results with $P_p = 10$ kPa appear on the bottom graphs.

The first pressure rise is practically the same both for ethanol and for acetaldehyde, even though it is slightly higher with ethanol. According to the Joukowsky equation, the pressure rise is a function of the liquid density and the speed of sound, together with the flow velocity ($\Delta P = \rho c v$). Both ethanol and acetaldehyde have nearly the same density and speed of sound measured with the ultrasonic transducer: $\rho = 789$ kg/m^3 and $c = 1176$ m/s for ethanol, and $\rho = 783$ kg/m^3 and $c = 1141$ m/s for acetaldehyde. Therefore, a similar pressure rise is expected with both liquids, and if it is slightly higher with ethanol, it is due to the higher speed of sound in this liquid. The highest pressure rise is obtained with water, in agreement with the higher values of density and speed of sound of this liquid: $\rho = 998$ kg/m^3 and $c = 1487$ m/s, measured with the ultrasonic transducer.

Regarding the flow velocity in the line, it can be estimated by the time occurrence of the first pressure peak. Here, ethanol and acetaldehyde reach the bottom end much faster ($t \approx 0.09$ s) than water does ($t \approx 0.12$ s). This is consistent with Navier–Stokes momentum equation, where the liquid front velocity is inversely proportional to $\overline{\rho}$. Therefore, liquid front velocity with ethanol and acetaldehyde is higher than with water, resulting in a faster arrival of the liquid front to the bottom end. On the other hand, the values of density and speed of sound in water are high enough to induce a higher pressure rise, despite the lower velocity of the liquid front.

It has already been mentioned that water gives nearly the same peak levels under deaerated and saturated conditions. Lower pressure peaks can be observed with saturated ethanol, and acetaldehyde displays the greatest differences between saturated and deaerated conditions. Once more, the pressure levels observed in Fig. 14 indicate that acetaldehyde appears to undergo a higher desorption rate when the pressure conditions in the liquid change, compared to the other two liquids.

Regarding the pressure attenuation, the signal attenuation pattern is highly affected by the gas release, that is why acetaldehyde, due to its high desorption rate, shows the fastest signal attenuation on the dimensionless graphs of Fig. 14. Under these circumstances, the fluid hammer attenuation process is mainly driven by the growing amount of NCG in the liquid + gas mixture, independently

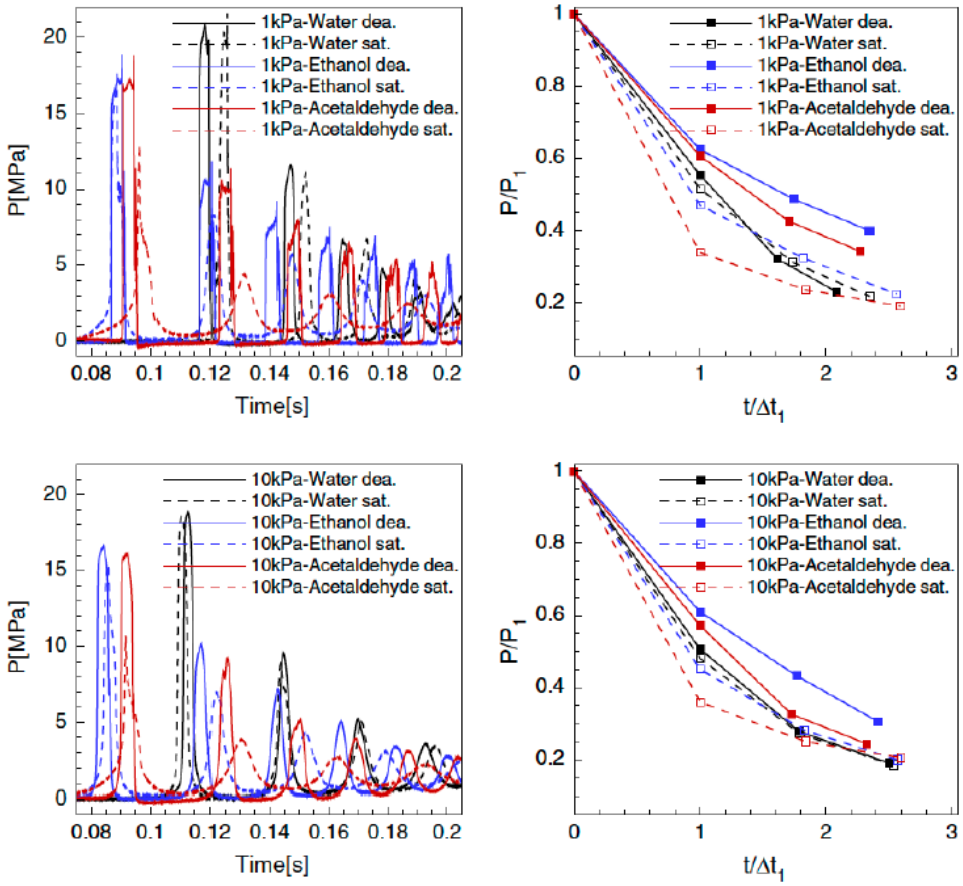

Fig. 14 Pressure evolution and dimensionless peak values obtained with the three liquids under deaerated and saturated conditions

of other physical properties mentioned under deaerated conditions. The pressure attenuation process for ethanol is also faster compared to the deaerated results. In the other extreme, the water attenuation pattern is almost unaffected by the saturated conditions, due to the slow desorption rate of this liquid.

As it was previously explained, the time reference is set by the trigger of the acquisition system, which is an imprecise method. In any case, there is a tendency in the occurrence of the first pressure peak; thus, in the first arrival of the liquid front to the bottom end, that has to be mentioned here. When $Pp = 10$ kP, the pressure raise is lower and takes place sooner than when $Pp = 1$ kP, and this is observed with the three liquids used, although it is more noticeable with water and ethanol. According to the Joukowsky equation, the higher the flow velocity, the higher the pressure rise, contrary to the results presented here. What is missing in this analysis is the cavitation in the FOV due to the initial pressure value in the line, which certainly creates a choked flow through the valve. Under these conditions, the flow remains constant, despite the continuous opening. Going back to the results presented for water and ethanol, when $Pp = 1$ kP the pressure in the line is below the vapor pressure of these two liquids. Therefore, flashing must take place without the opportunity to condense until the conditions in the line are above the vapor pressure. In case of $Pp = 10$ kP, if flashing occurs it will be during a shorter time, as this value is already above the vapor pressure of water and ethanol. As a consequence of this, the liquid flow through the valve will be established faster when the initial pressure in the line is higher, and the liquid front will reach the bottom end sooner. In case of acetaldehyde, both initial pressure conditions in the line are well below the vapor pressure of this liquid, and the chocked conditions in the valve will be similar. That is the reason why the first pressure peak with acetaldehyde takes place at the same time, no matter the initial pressure in the line. The study of cavitation in valves is out of the scope of the present study, but the two-phase flow taking place during the valve opening needs to be taken into account to understand the fluid hammer event in the line.

5 Conclusions

This paper describes experiments carried out to study the priming process in propulsion systems, with special attention to the gas desorption taking place during fluid hammer occurrence. For this purpose, it has been necessary to design and build a facility where the gas saturation level

of the test liquid can be controlled, which is achieved by using a spherical accumulator with a mounting membrane as pressuring tank.

The analysis of the experimental data is based on the pressure evolution and on the dimensionless peak levels. The attenuation is quantif ed by dividing the peak pressure by the amplitude of the f rst pressure rise and dividing the peak time occurrence by the resulting time delay between the f rst and second peaks. This dimensionless representation has proven to be an effective way to compare the pressure signal attenuation among different test conditions.

The f rst results with water allow concluding that the initial residual gas content in the line is responsible for attenuating the pressure rise due to its cushioning effect. Regarding the attenuation pattern, the higher is the initial f uid hammer pressure rise, the longer is the signal attenuation process. Results with saturated water are very similar to the ones obtained under deaerated conditions, in terms of both peak amplitude and signal decay. It appears that the desorption rate in this liquid is very slow, with minimal effect on the f uid hammer mechanism.

On the other hand, clear differences are observed when comparing pressure measurements obtained with deaerated and saturated ethanol. The differences are even more noticeable when acetaldehyde is the test liquid. These results are in agreement with the desorption rate deduced for the three liquids: acetaldehyde under saturated conditions undergoes a high desorption rate, a lower desorption rate occurs in ethanol, and water undergoes the lowest desorption rate of the three liquids. The desorbed NCG (noncondensable gas) increases the f uid compressibility, lowers the wave velocity, and thus reduces the pressure surges during f uid hammer occurrence. Finally, a high desorption rate offers a pressure attenuation process mainly driven by the gas release, with a minor inf uence of the residual gas initially present in the line.

The comparison of the results for the three liquids in the straight-line conf guration shows that, besides the desorption rate, density and speed of sound appear as the key liquid properties, without a clear inf uence of the vapor pressure on the f uid hammer phenomenon.

Acknowledgments The present research activity was initiated and promoted by the European Space Research and Technology Centre of the European Space Agency (ESTEC/ESA) through the GSTP activity AO/1-6210/09/NL/CP.

References

Abernethy RB, Benedict RP, Dowdell RB (1985) ASME measurement uncertainty. J Fluids Eng Trans Asme 107(2):161–164

Battino R, Rettich TR, Tominaga T (1984) The solubility of nitrogen and air in liquids. J Phys Chem Ref Data 13(2):563–600

Bergant A, Simpson AR, Tijsseling AS (2006) Water hammer with column separation: a historical review. J Fluids Struct 22:135–171

Castellan GW (1983) Physical chemistry, 3rd edn. Addison-Wesley Publishing Company, Reading

da Silva AB, de Freitas Rachid FB (2013) Modeling of release and absorption of gas in liquid–gas f ows within a consistent thermodynamic framework. Int J Eng Sci 66–67:21–43

Dieck RH (2007) Measurement uncertainty: methods and applications, 4th edn. ISA—The Instrumentation, Systems and Automation Society

Fischer K, Wilken M (2001) Experimental determination of oxygen and nitrogen solubility in organic solvents up to 10 Mpa at temperatures between 298 K and 398 K. J Chem Thermodyn 33:1285–1308

Katayama T, Nitta T (1976) Solubilities of hydrogen and nitrogen in alcohols and n-hexane. J Chem Eng Data 21(2):194–196

Kline SJ, McClintock FA (1953) Describing uncertainties in single-sample experiments. Mech Eng 1:3–8

Kranenburg C (1974) Gas release during transient cavitation in pipes. J Hydraul Div 100(10):1383–1398

Leca C, Boh P (2000) Mon and MMH pressure surges for a simplif ed propellant feed system. In: Proceedings of 3rd international conference on spacecraft propulsion. Cannes, France

Lin TY, Baker D (1995) Analysis and testing of propellant feed system priming process. J Propuls Power 11(3):505–512

Molinsky J (1997) Water hammer test of the SeaStar hydrazine propulsion system. In: 33rd AlAA/ASME/SAE/ASEE Joint Propulsion Conference & Exhibit

Morgan MJ (2004) Pressure transient characterization test for star-2 propulsion system fuel manifold. In: 40th AIAA/ASME/SAE/ASEE Joint Propulsion Conference and Exhibit

Ounougha L, Colozzi F (1997) Correlation between simulations and experiments on water hammer effect in a propulsion system. In: Proceedings of Second European Spacecraft Propulsion Conference

Prickett RP, Mayer E, Hermal J (1992) Water hammer in a spacecraft propellant feed system. J Propuls Power 8(3):592–597

Sander R (1999) Compilation of Henry's law constants for inorganic and organic species of potential importance in environmental chemistry. Tech. rep, Air Chemistry Department-Max-Planck Institute of Chemistry

Wilhelm E, Battino R, Wilcock RJ (1977) Low-pressure solubility of gases in liquid water. Chem Rev 77(2):219–262

Wylie EB, Streeter VL (1978) Fluid transients. McGraw-Hill Inc, New York

Yaggy KL (1984) Analysis of propellant f ow into evacuated and pressurized lines. In: 20th AIAA/SAE/ASME Joint Propulsion Conference and Exhibit